Helmholtz-Zentrum
hereon

Final Draft
of the original manuscript:

Mikhailau, A.; Maltanava, H.; Poznyak, S.K.; Salak, A.N.; Zheludkevich, M.L.; Yasakau, K.A.; Ferreira, M.G.S.:

One-step synthesis and growth mechanism of nitrate intercalated ZnAl LDH conversion coatings on zinc.

In: Chemical Communications : ChemComm. Vol. 55 (2019) 6878 - 6881.
First published online by Royal Society of Chemistry: 28.05.2019

https://dx.doi.org/10.1039/C9CC02571E

One-step synthesis and growth mechanism of nitrate intercalated ZnAl LDH conversion coatings on zinc

Aliaksandr Mikhailau, [a] Hanna Maltanava,[ab] Sergey K. Poznyak,[b] Andrei N. Salak, [a] Mikhail L. Zheludkevich,[c] Kiryl A. Yasakau*[a] and Mário G. S. Ferreira [a]

[a] *Department of Materials and Ceramics Engineering, CICECO – Aveiro Institute of Materials, University of Aveiro, 3810-193 Aveiro, Portugal. E-mail: kyasakau@ua.pt*
[b] *Research Institute for Physical Chemical Problems, Belarusian State University, 220030 Minsk, Belarus*
[c] *Magnesium Innovations Centre (MagIC), Helmholtz-Zentrum Geesthacht, Germany*

An approach for the synthesis of ZnAl–NO_3 LDH conversion coatings on zinc in an aqueous acidic $Al(NO_3)_3$/$NaNO_3$ solution is demonstrated for the first time. The growth mechanism has been investigated using time resolved structural, microstructural and analytical methods. A LDH growth model involving both electrochemical and chemical processes is suggested.

Layered double hydroxides (LDHs) or so called synthetic anionic clays, have gained considerable interest as they possess versatile potential applications.[1a] The general formula of most common LDHs is $[M_{1-x}^{2+}M_x^{3+}(OH^-)_2]^{x+}A_{x/n}^{n-}mH_2O$, where M^{2+} and M^{3+} are di- and trivalent metal cations respectively, A^{n-} is an anion, and x is equal to the molar ratio $M^{3+}/(M^{2+}+M^{3+})$ which usually is between 0.22 and 0.33.[1b] LDHs feature a layered structure derived from the stacking of positively charged brucite-type layers with anions in the interlayer space. Owing to the layered nature and peculiarities of chemical binding that combines both electrostatic and hydrogen-bound interactions, the interlayer species can be exchanged, preserved inside and released in a controlled manner.[1c] LDHs possess high flexibility of chemical composition having various combinations of metal ions, atomic ratios, and natures of the interlayer anions. This makes LDHs widely acceptable as functional materials and delivery nano-carriers in biomedicine,[1d] composite hydrogels[1e] photoluminescence,[1f] stimuli-responsive intelligent materials,[1g] polymer thermal stabilizers[1h] and corrosion protection.[1i]

Many studies use the coprecipitation method as the most facile way of preparing nano- and microstructured LDH particles.[1j] However, some applications require the LDH to be immobilized on a substrate. These demands inspired the fabrication of LDH coatings directly on different surfaces and started a trend of applying LDH-based devices for heterogeneous catalysts, clay- modified electrodes, sensors, photoanodes, and light emitters.[2] *In situ* LDH growth has been widely developed on pure aluminium, Al-based or Mg-based alloys and anodic aluminium oxide sub- strates to form LiAl, MgAl, NiAl, ZnCo or ZnAl LDH films.[3] A typical LDH conversion coating process involves a metallic (M1) substrate immersed in a solution of inorganic metal salt (M2) acting as a source of metal cations for LDH growth.[4] The solution may be heated and the synthesis can be carried out from several minutes to several days.[5] However, the direct growth of LDH with nitrates on zinc substrates remains a considerable challenge. Synthesis of carbonate substituted LDH films on zinc-based substrates was first introduced by Buchheit *et al.* and later by others.[6] Unfortunately, carbonate- or hydroxyl containing LDHs are quite stable and possess poor anionic exchange ability for other anions.[7] In contrast, nitrate containing LDHs appear to be among the best precursors for anion exchange reactions. LDH coatings would have great potential to be used as 'smart' functional surface treatments for zinc-based substrates like structural materials for biodegradable implants or the widely used galvanized steel.

In this work we present for the first time a method for preparing ZnAl–NO_3 LDH conversion coatings on metallic zinc. The method allows the synthesis of LDHs with incorporated nitrate anions in one step, without a secondary anion exchange process, which to our knowledge has not been reported. More- over in this work significant efforts have been made to under- stand the mechanism of LDH growth which uncovers the importance of chemical and electrochemical processes.

The LDH synthesis has been carried out in 1 mM $Al(NO_3)_3$ + 0.1 M $NaNO_3$ solution at 90 1C using pure zinc as a substrate. The obtained LDH conversion coating is uniform and well attached to the substrate. Fig. 1 and 2 depict the XRD patterns and SEM images of the samples after the synthesis for different periods of time. In all the XRD patterns, the diffraction reflec- tions from the zinc metal substrate were used as an internal standard and cut afterwards (a full XRD pattern is available in Fig. S1, ESI†). At the end of 20 h synthesis XRD data reveal three well-defined LDH phases with distinct values of the interlayer

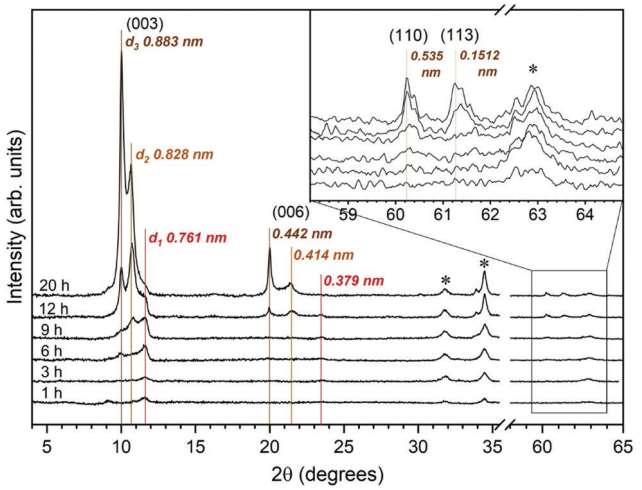

Fig. 1 Evolution of the XRD patterns of the Zn substrate after the synthesis for 1 h, 3 h, 6 h, 9 h, 12 h and 20 h in 1 mM $Al(NO_3)_3$ + 0.1 M $NaNO_3$ solution. Reflections corresponding to ZnO are denoted with an asterisk (*). Inset shows the high-angle ranges of the XRD patterns. The numbers (in italic) at the diffraction reflections correspond to the respective interplanar distances.

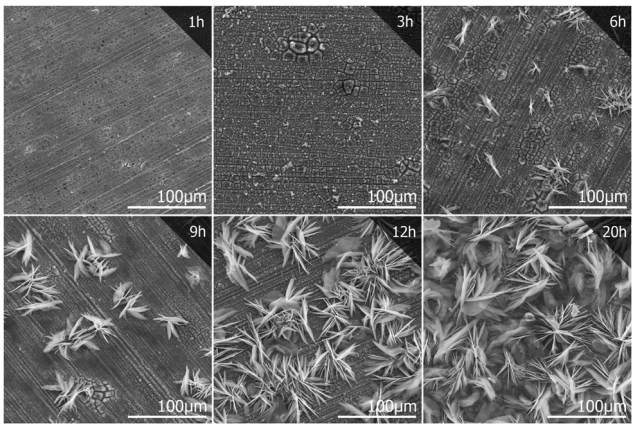

Fig. 2 SEM images of the zinc surface morphology after the synthesis treatment for 1–20 hours.

distances (basal spacing, d), namely d_1 = 0.761 nm, d_2 = 0.828 nm, and d_3 = 0.883 nm (Fig. 1). According to the observed values of the basal spacing, the first phase (hereafter, d_1-LDH phase) is suggested to be a ZnAl LDH, intercalated with either carbonate or hydroxide anions.[8a] FTIR analysis could not distinguish these two anions due to the low amount of the d_1 phase (Fig. S2, ESI†). The obtained FTIR spectra are typical for LDH-NO_3.[8b] The phase with the highest basal spacing value, namely d_3-LDH, corresponds well to a ZnAl LDH with a similar $Zn_{(II)}/Al_{(III)}$ cation ratio to that in the d_1-LDH phase, but intercalated with nitrate. The d_3 value is in good agreement with those observed in $Zn_{0.67}Al_{0.33}$–NO_3 LDH powders.[8c] The site symmetry of the nitrate anion found from the spectroscopic study indicates its tilted (against the layer plane) arrangement in the interlayer.[8c] As regards the d_2-LDH phase, one can suggest that the intercalated anion is NO_3^- while the tilt angle is smaller than that in the d_3-LDH phase. Nitrate anions are arranged at a smaller tilt angle if the layer charge per formula unit is smaller. An abrupt decrease of the basal spacing has been observed in $Mg_{1-x}Al_x$–NO_3 LDH[8d] when x was changed from about 0.30 to 0.22. Using the $d(x)$ dependence reported by Xu and Zeng[8d] and taking into account the values of thickness of Mg-based and Zn-based hydroxide layers, 0.477 and 0.471 nm, respectively,[8e] we consider that the composition of the d_2-LDH phase is close to $Zn_{0.75}Al_{0.25}$–NO_3. The total Zn/Al ratio determined by the analytical method is 2.21 ± 0.05 which is in accordance with those values suggested by XRD and corresponds to the average composition between d_2 and d_3 phases being $Zn_{0.69}Al_{0.31}$–NO_3. In addition to the diffraction peaks of the described three LDH phases, the reflections attributed to a wurtzite ZnO phase (JCPDS card # 36-1451) are also observed in the XRD patterns (Fig. 1).

The growth of different LDH phases starts at different times of synthesis. Initially, the d_1 phase appears, followed by the d_2 phase. After 6 h of synthesis the d_3-phase appears, and this phase becomes predominant after 20 h (Fig. 1). Such kinetics suggests that the growth conditions during the synthesis gradually change and this point is further addressed below.

SEM micrographs presented in Fig. 2 describe the surface changes of zinc after different times of synthesis. During the first 3 hours of synthesis the substrate is covered with a film having a mudcrack pattern (Fig. 2). The EDS spectrum taken from the cracked coating after 1 hour of treatment reveals the significant aluminum content on the

surface (Fig. S3a and c, ESI†). This evidences the deposition of preferably amorphous aluminum hydroxide on the zinc surface. Such aluminum hydroxide can strongly affect the rate of zinc dissolution and the LDH formation kinetics. The micrographs taken at higher magnification illustrate well developed cracks in the film. Hexagonal crystals of ZnO (Fig. S4, ESI†) are well distinguishable in the cracks at the beginning of the synthesis, which coincide with XRD studies (Fig. 1). Zinc oxide is interweaved with the network of crystals in the cracks of the coating (Fig. S5a, ESI†). These crystals may correspond to the d_1-LDH phase, reported above, and can serve as nucleation centers supporting the growth of the d_2- and d_3-LDH phases (Fig. S5b, ESI†).

After 6 hours of treatment there is a noticeable growth of LDH, and by the end of 20 hours the LDH film almost entirely covers the substrate (Fig. 2) and the EDS spectrum (20 h) reveals the lower Al content (Fig. S3b and d, ESI†). As the time of treatment increases, the size and the thickness of the LDH crystals increase accordingly. The lateral size of the LDH platelets appears to be bigger (10–50 mm) than the size of platelets reported in other studies.[5a,6a,b] Moreover, the crystals are oriented out of the substrate plane, evidencing the conventional crystal growth mechanism from a solution[9a] and refuting the cation incorporation mechanism suggested in some studies.[9b] If the crystals were formed by incorporation of Me cations into a crystal lattice of aluminum hydroxide or boehmite, they would grow only in that layer and stay in the plane of the substrate. The growth process observed in this work occurs through the formation of small terraces on the LDH platelets (Fig. S6, ESI†). Such morphology suggests the layer-by-layer crystal growth process,[9a]

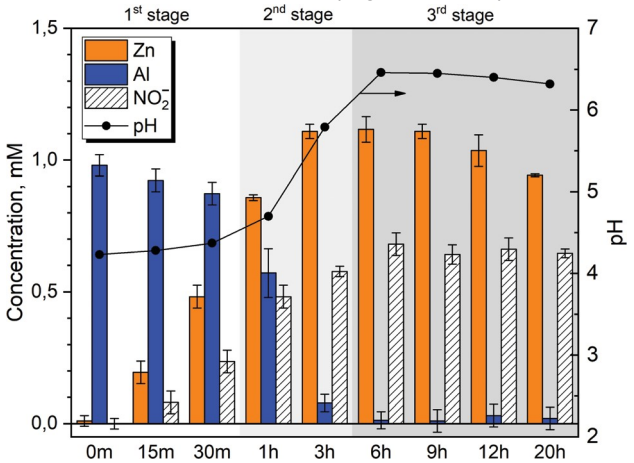

Fig. 3 The time-resolved evolution of Al, Zn and NO_2^- concentrations in the solution and its pH (measured at 25 1C) after different times of synthesis.

in contrast to the dislocation-driven growth which has been observed by Forticaux *et al.*[9c]

The growth kinetics has been further studied by looking at the changes of concentrations of different species in the solution during the synthesis. Fig. 3 displays the general trend of the changes of total Al and Zn concentration in the electro- lyte with time along with the solution pH. The overall kinetics may be divided into three stages. The first stage is relatively fast and occurs during the first hour of the treatment. At that stage the zinc concentration rapidly increases, and aluminum concentration slightly decreases (Fig. 3). In an aqueous solution containing metallic zinc and nitrate anions several electrochemical processes involving anodic dissolution of zinc (1) and cathodic reduction of nitrates and oxygen (2) and (3) can occur. The cathodic processes generate hydroxyl ions and create a pH gradient.[10] The concentration of nitrite anions in the solution, determined by permanganometric titration,[11] increases with time (Fig. 3). Although the reduction of nitrates to nitrite has been proven, there are other possible reactions involving nitrate and nitrite anions, producing nitrogen gas or ammonia, which may contribute to the overall reduction process.[10] Fig. 4 schematically presents the first stage of the LDH growth mechanism involving the main electro- chemical reactions.

$$Zn^{2+} + 2e^- \rightarrow Zn \quad (1)$$

$$NO_3^- + H_2O + 2e^- \rightarrow NO_2^- + 2OH^- \quad (2)$$

$$O_2 + 2H_2O + 4e^- \rightarrow 4OH^- \quad (3)$$

Although reactions (2) and (3) produce hydroxyl anions, the pH of the bulk solution does not sufficiently change (Fig. 3). This can be rationalized by the hydrolysis equilibrium of aluminum ions buffering the pH (4) and (5):

$$Al^{3+} + OH^- \rightleftharpoons Al(OH)^{2+}; \quad Al(OH)^{2+} + OH^- \rightleftharpoons Al(OH)_2^+ \quad (4)$$

$$Al(OH)_2^+ + OH^- \rightarrow Al(OH)_3\downarrow \quad (5)$$

When the buffering capacity of aluminum containing species is exhausted, aluminum hydroxide starts to precipitate

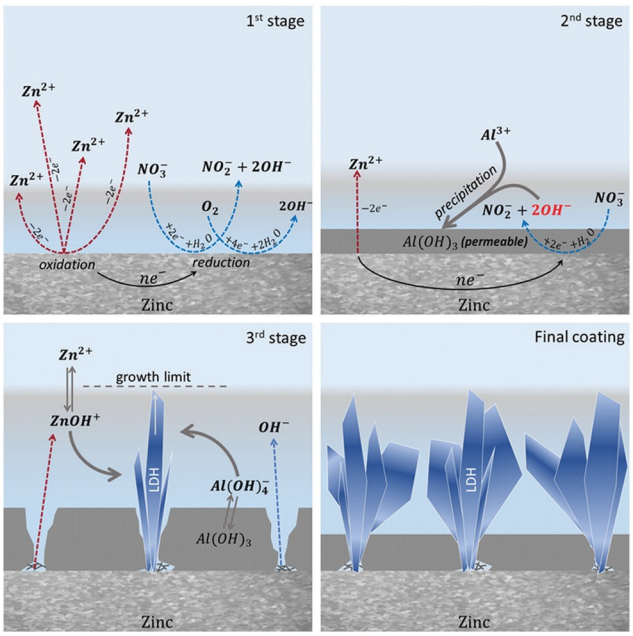

Fig. 4 The scheme of the proposed mechanism of LDH growth on zinc in the solution of 0.1 M $NaNO_3$ + 1 mM $Al(NO_3)_3$.

on the Zn substrate owing to the higher pH near the surface. This indicates the beginning of the second stage of LDH growth (Fig. 4). During this stage (Fig. 3) the concentration of Al in the solution decreases and that of Zn increases, while the pH grows due to the active electrochemical reduction reactions. At this stage (1–6 h) XRD analysis revealed the presence of the d_1 phase. This phase may have a lower $Zn_{(II)}/Al_{(III)}$ ratio than the other two phases due to presumably higher concentration of soluble Al species and higher local pH at the surface.

The third stage begins with an active phase of LDH growth when soluble aluminum has mainly precipitated as a hydroxide on the zinc surface (Fig. 3 and 4). The formed coating acts as a diffusion barrier slowing down the zinc dissolution process. There are no significant changes in zinc and aluminum con- centrations and pH during this stage. The concentrations of species and pH at the zinc surface are apparently favorable for LDH growth. The growth occurs *via* the conventional solution crystal growth.[9a] LDH nucleation occurs in cracks of the coating (Fig. S5b, ESI†), and the micro-scale network inside the cracks presumably serves as a nucleation center for the main LDH phases (d_2 and d_3). Next, soluble zinc and aluminum species build LDH crystals at a sufficiently high pH. The slight drop of zinc concentration and almost stable pH during the last stage (Fig. 3) may be explained by active growth of LDH consuming zinc and hydroxyl species.

The distribution of various species of Al and Zn during the synthesis process may be scrutinized with the help of a Pourbaix diagram (Fig. S7, ESI†). The latter was constructed regarding the conditions of the synthesis such as temperature
90 1C and pressure 1 bar, and plausible concentrations of Al and Zn being 0.05 mM and 1 mM respectively determined by the analytical method. At the beginning of the synthesis the bulk solution pH was about 3.3 (measured at 90 1C) at which mostly soluble Al^{3+} and Zn^{2+} species exist (Fig. S6, ESI†). Then the pH gradually increases, which induces the precipitation of aluminum hydroxide which is stable in the pH region 4.4 to 6 (at 90 1C) (Fig. S6a, ESI†). Electrochemical processes keep the pH at the zinc surface higher (~6) compared to what has been measured at the end of the synthesis in the bulk solution, *i.e.*,
5.9 (at 90 1C). This is consistent with the growth of the ZnO phase during the treatment process (Fig. 1), and the pH stability border of the ZnO phase is more than 6.2 (at 90 1C) (Fig. S6b, ESI†). At the higher pH, $Al(OH)_3$ dissolves forming $Al(OH)_4^-$ species (Fig. S6, ESI†) which, alongside the $ZnOH^+$ ones, act as the LDH building blocks as schematically shown in Fig. 4. The LDH growth depends on the transport of these species and on the pH, which must be in the stability range of LDH. These are the factors that ultimately limit the growth process (Fig. 4).

It must be stressed that the equilibria of species and pH are different in the vicinity of the substrate surface compared to the bulk solution. Despite the low concentration of aluminum species in the bulk solution, LDH phases actively grow (Fig. 1 and 2). The $Zn_{(II)}/Al_{(III)}$ ratio in the two main LDH phases (d_2 and d_3) is different according to XRD results. Such discre- pancy may occur when there is dispersion in the concentration of soluble Al and Zn species at the surface influencing the cation ratio in the LDH phases.

In summary, ZnAl–NO_3 LDH has been synthesized *in situ* on
a zinc surface. Unlike other studies, the proposed method allows the production of LDH intercalated with nitrate as the counter anion in one step without an additional anionic exchange stage. Explicit evidence was provided to reveal the growth mechanism which involves key steps such as nitrate anion reduction and zinc oxidation reactions along with aluminum hydroxide deposition followed by reprecipitation of $Al(OH)_4^-$ and $ZnOH^+$ species into the LDH phases.

Electro- chemical reactions are vital for successful LDH synthesis on zinc and must be paid a great deal of attention to design other LDH functional films on different metallic substrates. Applica- tions of LDH coatings on zinc extend but are not limited to self- healing coatings, scavenging of aggressive anions, sensing of anionic species and onset of degradation of coatings. The proposed method, as well as the mechanism, will stimulate future studies designing tailored LDH coatings on other zinc- based substrates such as zinc galvanized steel, Zn–Al–Mg galvanized coatings, and, to some extent, on other metallic substrates.

KY acknowledges a researcher grant (IF/01284/2015). The authors acknowledge project CICECO-Aveiro Institute of Materials and FCT Ref. UID/CTM/50011/2019, financed by national funds through the FCT/MCTES. This research received funding from the European Union's Horizon 2020 research and innovation programme under the Marie Skłodowska-Curie grant agreement no. 645676, project MULTISURF.

Conflicts of interest

There are no conflicts to declare.

References

1 (*a*) F. Cavani, F. Trifirò and A. Vaccari, *Catal. Today*, 1991, 11, 173–301; (*b*) R. Xu, W. Pang and Q. Huo, *Modern Inorganic Synthetic Chemistry*, Elsevier Science, 2011; (*c*) A. I. Khan, L. Lei, A. J. Norquist and D. O'Hare, *Chem. Commun.*, 2001, 2342–2343; (*d*) X. Mei, R. Liang, L. Peng, T. Hu and M. Wei, *J. Mater. Chem. B*, 2017, 5, 3212–3216; (*e*) Z. Hu and G. Chen, *Adv. Mater.*, 2014, 26, 5950–5956; (*f*) L. Wu, G. Chen and Z. Li, *Small*, 2017, 13, 1–7; (*g*) Y. Zhao, H. Lin, M. Chen and D. Yan, *Ind. Eng. Chem. Res.*, 2014, 53, 3140–3147; (*h*) J. Liu, G. Chen and J. Yang, *Polymer*, 2008, 49, 3923–3927; (*i*) A. Lutz, O. van den Berg, J. Wielant, I. De Graeve and H. Terryn, *Front. Mater.*, 2016, 2, 73; (*j*) K. A. Carrado, A. Kostapapas and S. L. Suib, *Solid State Ionics*, 1988, 26, 77–86.

2 (*a*) X. Guo, F. Zhang, D. G. Evans and X. Duan, *Chem. Commun.*, 2010, 46, 5197–5210; (*b*) Y. Tang, R. Wang, Y. Yang, D. Yan and X. Xiang, *ACS Appl. Mater. Interfaces*, 2016, 8, 19446–19455; (*c*) D. Yan, J. Lu, L. Chen, S. Qin, J. Ma, M. Wei, D. G. Evans and X. Duan, *Chem. Commun.*, 2010, 46, 5912–5914; (*d*) R. Gao and D. Yan, *Chem. Commun.*, 2017, 53, 5408–5411.

3 (*a*) H. Chen, F. Zhang, S. Fu and X. Duan, *Adv. Mater.*, 2006, 18, 3089–3093; (*b*) K. A. Yasakau, A. Kuznetsova, S. Kallip, M. Starykevich, J. Tedim, M. G. S. Ferreira and M. L. Zheludkevich, *Corros. Sci.*, 2018, 143, 299–313; (*c*) J. Chen, Y. Song, D. Shan and E.-H. Han, *J. Mater. Sci. Technol.*, 2015, 31, 384–390; (*d*) T. N. Shulha, M. Serdechnova, S. V. Lamaka, D. C. F. Wieland, K. N. Lapko and M. L. Zheludkevich, *Sci. Rep.*, 2018, 8, 16409; (*e*) Y. Zhang, J. Liu, Y. Li, M. Yu, S. Li and B. Xue, *J. Coat. Technol. Res.*, 2015, 12, 595–601; (*f*) L. Xue, Y. Cheng, X. Sun, Z. Zhou, X. Xiao, Z. Hu and X. Liu, *Chem. Commun.*, 2014, 50, 2301–2303; (*g*) P. Ramakul, M. Hronec and U. Pancharoen, *Korean J. Chem. Eng.*, 2007, 24, 282–287; (*h*) Y. Li, L. Zhang, X. Xiang, D. Yan and F. Li, *J. Mater. Chem. A*, 2014, 2, 13250–13258.

4 (*a*) J. Tedim, M. L. Zheludkevich, A. N. Salak, A. Lisenkov and M. G. S. Ferreira, *J. Mater. Chem.*, 2011, 21, 15464–15470; (*b*) A. N. Salak, A. D. Lisenkov, M. L. Zheludkevich and M. G. S. Ferreira, *ECS Electrochem. Lett.*, 2014, 3, C9–C11.

5 (*a*) J.-K. Lin, J.-Y. Uan, C.-P. Wu and H.-H. Huang, *J. Mater. Chem.*, 2011, 21, 5011; (*b*) X. Guo, S. Xu, L. Zhao, W. Lu, F. Zhang, D. G. Evans and X. Duan, *Langmuir*, 2009, 25, 9894–9897.

6 (*a*) R. G. Buchheit and H. Guan, *JCT Res.*, 2004, 1, 277–290; (b) K. Hoshino, S. Furuya and R. G. Buchheit, *J. Electrochem. Soc.*, 2018, 165, C461–C468; (*c*) J. Liu, Y. Li, X. Huang, G. Li and Z. Li, *Adv. Funct. Mater.*, 2008, 18, 1448–1458.

7 (*a*) D. G. Costa, A. B. Rocha, W. F. Souza, S. S. X. Chiaro and A. A. Leitão, *Appl. Clay Sci.*, 2012, 56, 16–22; (*b*) S. Miyata, *Clays Clay Min.*, 1983, 31, 305–311.

8 (*a*) M. Serdechnova, A. N. Salak, F. S. Barbosa, D. E. L. Vieira, J. Tedim, M. L. Zheludkevich and M. G. S. Ferreira, *J. Solid State Chem.*, 2016, 233, 158–165; (*b*) W. Kagunya, R. Baddour-Hadjean, F. Kooli and W. Jones, *Chem. Phys.*, 1998, 236, 225–234; (*c*) A. N. Salak, J. Tedim, A. I. Kuznetsova, J. L. Ribeiro, L. G. Vieira, M. L. Zheludkevich and M. G. S. Ferreira, *Chem. Phys.*, 2012, 397, 102–108; (*d*) Z. P. Xu and H. C. Zeng, *J. Phys. Chem. B*, 2001, 105, 1743–1749; (*e*) G. W. Brindley and C.-C. Kao, *Phys. Chem. Miner.*, 1984, 10, 187–191.

9 (*a*) A. Holden and P. Morrison, *Crystals and crystal growing*, MIT Press, 1982; (*b*) Z. Meng, Y. Zhang, Q. Zhang, X. Chen, L. Liu, S. Komarneni and F. Lv, *Appl. Surf. Sci.*, 2017, 396, 799–803; (c) A. Forticaux, L. Dang, H. Liang and S. Jin, *Nano Lett.*, 2015, 15, 3403–3409.

10 (*a*) C. Polatides and G. Kyriacou, *J. Appl. Electrochem.*, 2005, 35, 421–427; (*b*) J. Ding, W. Li, Q.-L. Zhao, K. Wang, Z. Zheng and Y.-Z. Gao, *Chem. Eng. J.*, 2015, 271, 252–259.

11 J. Rosin, *Reagent chemicals and standards*, LWW, 1955, vol. 79.